

# Elastic/plastic indentation hardness and indentation fracture toughness: the inclusion core model

K. TANAKA

*Department of Mechanical Engineering, Technological University of Nagaoka, Nagaoka, Niigata 949-54, Japan*

A new model for determining elastic/plastic indentation is presented. This model generalizes Johnson's incompressible core model to a compressible material and allows the indentation pressure to be transmitted via a misfitted inclusion core beneath the indenter which is surrounded by a hemispherical plastic zone. The internal stress field inside the core is obtained by applying Eshelby's spherical inclusion problem together with Hill's spherical-cavity expansion analysis. The plastic deformation considered here exactly ensures compatibility between the volume of a material displaced by the indenter and that accommodated by expansion. The analysis explains the essential relationships between the dimensions of the indentation and plastic zone and the dominant material properties; yield stress, hardness and elastic modulus. The solution is extended to evaluate the indentation fracture toughness by taking into account the reduced half-space constraint by the image force.

## 1. Introduction

Indentation fracture is now established as a simple but important technique for determining the fracture toughness of ceramics. Its application stems from recent analysis of elastic/plastic indentation fracture, which is based on the evaluation of internal stress (residual stress) resulting from a misfit between the plastic zone beneath the indentation and the surrounding elastic matrix [1-7]. Particularly notable progress was developed in a series of works by Lawn, Evans and Marshall [1-5]. They calculated the elastic/plastic stress field treating the indentation pressure as a pressurized spherical cavity and applying Hill's spherical-cavity expansion solution. They offered a correlation between fracture toughness and  $P/a^{3/2}$ , where  $P$  is the indentation load and  $a$  the radius of a half-penny median crack [8]. However, they did not analytically obtain the correlation factor, but they semi-empirically determined it by comparing the indentation-determined toughness values with the conventional ones. Furthermore, it seems that their model has a difficulty in the correlation between the conventional hardness and the indentation pressure. Namely, they assumed that the volume of the cavity is equal to the Vickers indentation volume, so that the diameter of the spherical cavity is much smaller than the indentation diagonal.

Johnson [9] attempted to account for the influence of an indenter angle by allowing the indentation pressure to be transmitted via an incompressible hydrostatic core beneath the indenter and replace the cavity in Hill's model. Then, Johnson extended Hill's theory to obtain the elastic/plastic stress field outside the core ensuring compatibility between the volume of the material displaced by the indenter and that accom-

modated by expansion. However, the analysis gives a considerable underestimate for indentation measurements [9], and the estimate of the plastic zone radius *vis-à-vis* the core radius is particularly disparate [4]. Recently, Tanaka and co-workers [6, 7] proposed a new model based on the analogy of the internal spherical inclusion problem [10, 11]. The indentation volume was assumed to be accommodated by the transformation of a spherical inclusion beneath the indenter, which corresponds to the introduction of dislocations in the plastic zone beneath the indentation [7]. The theoretical prediction of the indentation toughness equation for well-developed cracks agreed excellently with the empirical one derived by Antis *et al.* [3]. However, the elastic/plastic stress field outside the indented area in the model did not satisfy the yielding condition of a material.

The present approach attempts to generalize Johnson's model by allowing the indentation pressure to be transmitted via a misfitted inclusion beneath the indenter (inclusion core model) and by adding a term related to the dissipated plastic work in the core. In contrast to Johnson's model, the core in this analysis is compressible and partially accommodates the volume of the material displaced by the indenter. The solution is applied to evaluate the correlation factor in the indentation fracture toughness equation. This takes into account the reduced half-space constraint or the image force contribution due to the presence of a free surface.

## 2. Indentation analysis

### 2.1. Basic model

The procedure is similar to those adopted by Johnson [9] and Lawn *et al.* [2]. Fig. 1 outlines the model. The

hemispherical plastic zone just underneath the indenter is taken to support the indenter over the characteristic contact radius  $c_1$ . Because of the constraint of the surrounding elastic material, the plastic deformation induces internal stresses and the plastic zone acts as a compressible hydrostatic core of pressure  $p_1$ . The surface area of the core,  $\pi c_1^2$ , is assumed to be equal to that of the indented area,  $2c^2$ , where  $c$  is half the indenter diagonal. Hence  $c_1 \cong 0.8c$ . The operation of the pressure  $p_1$  over the core wall creates a hemispherical plastic zone, radius  $b$ , outside the core. The latter situation is similar to that for a spherical cavity under a pressure  $p_1$ . Invariance of the indentation pressure in hardness measurements requires that the plastic zone volume be governed exclusively by the indentation volume [9]. It follows from this that the indentation volume  $\Delta V$  be compensated by the misfit induced in the total plastic zone. For a Vickers indenter, the included angle  $2\psi (= 136^\circ)$ ,

$$\Delta V = 2^{1/2} c^3 \cot \psi / 3 \quad (1)$$

The volume should be shared by the misfit volume in the plastic core,  $\Delta V_1$ , and that in the plastic zone outside the core,  $\Delta V_2$ .

To evaluate the internal stress field the following sequence of hypothetical operations is performed on the analogy with the internal spherical inclusion problem [10]. (1) Begin with an unstressed elastic half space and remove a segment of material with radius  $c_1$  (core) from the prospective contact site. (2) Apply an average pressure  $p_0$  to the prospective contact surface of the removed core and plastically deform it to allow a uniform expansion of misfit strain,  $\Delta V/V_1$ , where  $V_1$  is the volume of the removed core ( $= 2\pi c_1^3/3$ ). Then unload the pressure and hold it stress-free. (3) Apply a pressure  $p_2$  to the wall of the hole in the matrix to generate a plastic zone of radius of  $b$  around the hole, and relax the pressure. If  $\Delta V_2$  is the resulting volume change, Hill's expanding cavity analysis [8] gives the following form (see Appendix 1),

$$\Delta V_2/V_1 = [3Y(1 - \nu)/E](b/c_1)^3 - [9p_2(1 - \nu)/2E], \quad (2)$$

where  $Y$  is the yield stress,  $E$  is the Young's modulus, and  $\nu$  is the Poisson's ratio. The pressure  $p_2$  is related

to the yield stress as

$$p_2 = (2Y/3)[1 + 3 \ln (b/c_1)] \quad (3)$$

(4) Elastically restore the removed core to the radius of the expanded cavity by a hydrostatic compression across the outer boundary. Then reinsert the pressurized core into the expanded cavity, restoring coherence at the interface, and allow the system to relax elastically. Applying Eshelby's inclusion problem [10, 11], the resulting pressure  $p_1$  in the core can be related to the irreversible misfitted volume  $\Delta V_1 (= \Delta V - \Delta V_2)$  as

$$p_1 = [2E/9(1 - \nu)](\Delta V_1/V_1). \quad (4)$$

Hence, the internal stress satisfying the model outlined in Fig. 1 is obtained when

$$p_2 = p_1 \quad (5)$$

Using this condition and Equations 1 to 4, the plastic zone size  $b$  can be correlated with the yield stress in a functional form,

$$Y/E = [\cot \psi / 3 \times 2^{1/2} \pi (1 - \nu)] (c/b)^3 \quad (6)$$

The problem is the evaluation of the average pressure  $p_0$  at stage 2. This is related to the plastic work dissipated to heat in the core and not yet exactly solved, but may be written by

$$p_0 = \alpha Y \quad (7)$$

where  $\alpha$  is a material constant. The constant would be dependent on the deformation process in the core and estimated for the two extreme cases. The upper limit would be one, as derived from the case when a medium of depth  $c_1$  is pressed by a smooth flat die of width  $2c_1$  (Hill [8] p. 257). The lower limit would correspond to the case of the expansion of a plastic hemispherical shell with outer radius  $c_1$  (Hill [8] p. 99). In this case the volume of the inner cavity may be equalized to  $\Delta V$ . The pressure applied at the inner cavity wall is given by  $2Y \ln (c_1/c')$ , where  $c'$  is the inner radius and equal to  $0.45c$ . Hence the applied pressure averaged over the prospective indenter-contact surface becomes  $2\pi c'^2 Y \ln (c_1/c') / \pi c_1^2$ . This yields  $\alpha \cong 0.36$ . Therefore, the parameter  $\alpha$  would lie between 0.3 and 1.

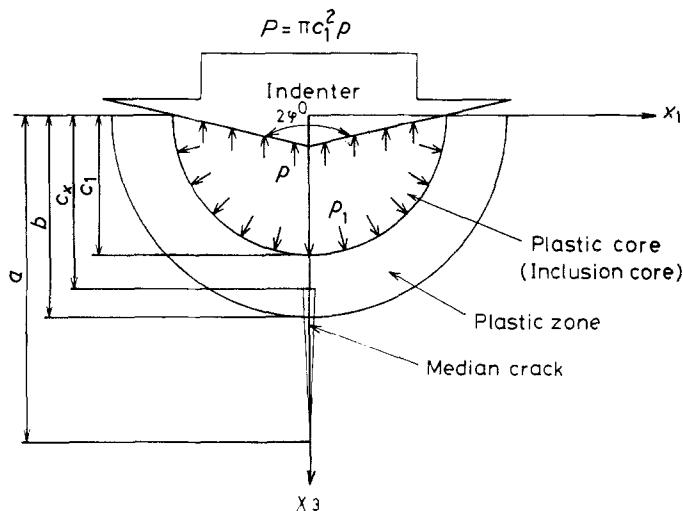


Figure 1 Schematic representation of elastic/plastic indentation.

The total pressure  $p$  is the sum of the residual pressure  $p_1$  and the pressure required for the plastic deformation in the core  $p_0$ , and it should be balanced with the applied load  $P$ . This is correlated with the conventional Vickers hardness  $H_v$ ,

$$H_v/\sin \psi = p = p_1 + \alpha Y. \quad (8)$$

Eliminating  $Y$  from Equation 8 in use of Equations 3 to 6, one obtains

$$E/H_v = [9\pi(1 - \nu)/2^{1/2} \cos \psi] \times (b/c)^3/[1 + 3\alpha/2 + 3 \ln(b/c_1)] \quad (9)$$

The solution is valid in the region where  $b \geq c_1$ . This condition gives

$$E/H_v \geq 9\pi(1 - \nu)2^{1/2}(1 + 3\alpha/2) \cos \psi \quad (10)$$

Eliminating  $b/c$  from Equations 3, 6 and 8, one determines the total pressure in the core and the hardness as a function of the ratio  $E/Y$ ,

$$\begin{aligned} p/Y &= H_v/Y \sin \psi = (2/3)[1 + 3\alpha/2 + 3 \ln(b/c_1)] \\ &= (2/3)\{1 + 3\alpha/2 \\ &\quad + \ln[E\pi^{1/2} \cot \psi/12(1 - \nu)Y]\} \end{aligned} \quad (11)$$

Johnson [9] obtained the following relations corresponding to Equations 11 and 6, respectively,

$$p/Y = (2/3)[1 + 3 \ln(b/c)] \quad (12)$$

$$(E/Y) \cot \psi = 6(1 - \nu)(b/c)^3 - 4(1 - 2\nu) \quad (13)$$

(although the definition of  $c$  in his paper is not clear). It is evident that Johnson's model is correct for special situations; Equation 12 is coincident with Equation 11 when the contribution from the dissipative plastic work in the core is neglected ( $\alpha = 0$ ), and Equation 13 becomes identical in form to Equation 6 in an extreme case of incompressible material ( $\nu = 0.5$ ).

## 2.2. Stress intensity factors

The present analysis calculates the residual term at an unloaded state in the case of a well-developed median crack of half-penny shape with a radius  $a$ . The detailed procedures for the calculation of stress intensity factors were described in previous papers [6, 12]. The coordinate system is shown in Fig. 1. It is assumed that the crack plane is open in the region where a radial location  $r$  is larger than  $c_x$  ( $c_x \leq r \leq a$ ). The stress intensity factor  $K$  averaged over the full angular range of the crack front can be represented by [12]

$$K = 2(a/\pi)^{1/2} \int_{\eta_x}^1 \bar{\sigma}_{22}(\xi) \xi d\xi / (1 - \xi^2)^{1/2} \quad (14)$$

where  $\xi = r/a$  and  $\eta_x = c_x/a$ .  $\bar{\sigma}_{22}(r)$  is the stress normal to the prospective crack plane ( $x_2 = 0$ ) at a radial location  $r$  from the crack centre averaged over the full angular range. This stress can be separated into the components as

$$\bar{\sigma}_{22}(r) = \bar{\sigma}_{22}^{\infty}(r) + \bar{\sigma}_{22}^{\text{im}}(r), \quad (15)$$

where  $\bar{\sigma}_{ij}(r)$  is the stress component in an infinite body

and  $\bar{\sigma}_{ij}^{\text{im}}(r)$  the image stress component due to the presence of a free surface. In correspondence with the two stress components, the relevant stress intensity factors  $K^{\infty}$  and  $K^{\text{im}}$  can be separately computed,

$$K = K^{\infty} + K^{\text{im}} \quad (16)$$

The stress intensity factors vary with the crack opening location  $c_x$ . It has been found that the value of  $K$  becomes maximum when  $c_x$  positions within the plastic zone outside the core ( $c_1 \leq c_x \leq b$ ). Hence, for simplicity, only the analytical results for the region will be represented in the following.

The spherical cavity solution [8] gives the stress distribution in an infinite body on the crack plane ( $x_2 = 0$ ),  $\bar{\sigma}_{22}^{\infty}$ , and on the half plane surface ( $x_3 = 0$ ),  $\bar{\sigma}_{33}^{\infty}$ :

$$\begin{aligned} \bar{\sigma}_{22}^{\infty}(r) &= \bar{\sigma}_{33}^{\infty}(r) = -p_1, & r < c_1 \\ \bar{\sigma}_{22}^{\infty}(r) &= \bar{\sigma}_{33}^{\infty}(r) = Y[(1/3) - 2 \ln(b/r)], & c_1 \leq r \leq b \\ \bar{\sigma}_{22}^{\infty}(r) &= \bar{\sigma}_{33}^{\infty}(r) = (Y/3)(b/r)^3, & r > b \end{aligned} \quad (17)$$

Integration of Equation 14 in the use of Equations 3, 5, 8 and 17 yields the stress intensity factor appropriate to an infinite body  $K^{\infty}$  for well-developed cracks ( $a \gg b$ ) as

$$\begin{aligned} K^{\infty} &= [P/(\pi a)^{3/2}](c_x/c_1)^2 \\ &\quad \times [1 + 3 \ln(b/c_x)]/[1 + 3\alpha/2 + 3 \ln(b/c_1)] \end{aligned} \quad (18)$$

The image stress  $\bar{\sigma}_{22}^{\text{im}}(r)$  is provided by the application of the traction  $-\bar{\sigma}_{33}^{\infty}(r)$  on the half plane surface. This can be determined using the Green's function for the semi-infinite body obtained by Mindlin [13] (see also [4, 14]). However, the analysis is so complicated that the exact integration is actually impossible. Thus the relevant image stress is approximately obtained as described in Appendix 2. This is given by

$$\bar{\sigma}_{22}^{\text{im}}(r) = \int_0^{\infty} \bar{\sigma}_{33}^{\infty}(\varrho) f(r/\varrho) d\varrho / \pi \varrho \quad (19)$$

where  $f(r/\varrho)$  is a polynomial function of  $r/\varrho$  as expressed by Equation A7. Substitution of Equation 19 into Equation 14 and the integration for the condition that  $a \gg b$  results in  $K^{\text{im}}$ .

$$\begin{aligned} K &= [P/(\pi a)^{3/2}][1 + 3 \ln(b/c_1)] \\ &\quad \times g(c_x/c_1, b/c_1)/[1 + 3\alpha/2 + 3 \ln(b/c_1)], \end{aligned} \quad (20)$$

where  $g(c_x/c_1, b/c_1)$  is a polynomial function of  $c_x/c_1$  and  $b/c_1$ .

## 3. Analytical results and discussion

### 3.1. The hardness

Equation 11 is evaluated varying  $\alpha$  in four levels 0, 1/3, 2/3 and 1 for  $\nu = 0.25$  and the results are plotted by the respective solid lines in Fig. 2 in comparison with indentation measurements. The main experimental data for metal and polymer are those for Vickers pyramid by Marsh [15], and Hirst and Howse [16].

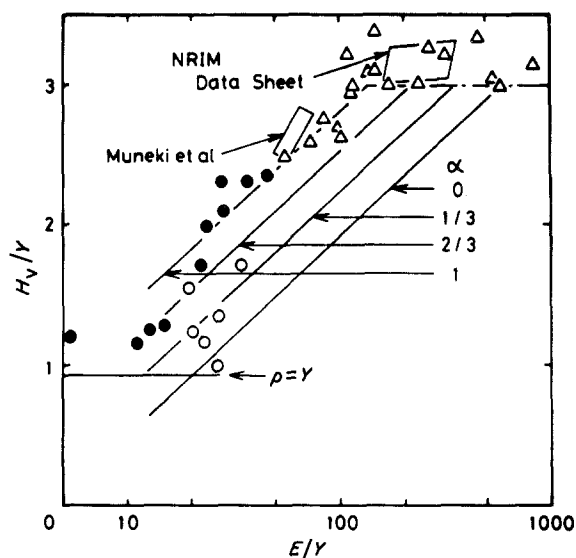


Figure 2 Literature data for experimental results on the ratio of the indentation pressure to the yield stress against the modulus to yield stress ratio for a range of materials. Also shown are the predictions in the present analysis for four  $\alpha$ -values ( $\nu = 0.25$ ). ( $\Delta$ ) Metal, ( $\circ$ ) ceramic, ( $\bullet$ ) polymer.

The additional ones are from Nishijima for various steels [17] and aluminium alloys [18]. The zone indicated by NRIM Data Sheet is from data of more than 200 steels [19]. Similarly, the zone of Muneki *et al.* is from data of 19 maraging steels [20]. When the data in references [17–20] are plotted,  $Y$  is, for convenience, taken as the tensile strength for the case of steels and the mean of tensile strength and 0.2% proof stress for the case of aluminium alloys. The detailed data for ceramics [3, 15, 21, 22] are shown in Table I. Usually the yield stress of ceramics is not available for bulk specimens. Hence the tensile strengths of whisker [21] and fibre [15] are taken for  $Y$ .

In the case of metals and polymers, at the larger  $E/Y$  region the experimental  $H_v/Y$  values become independent of  $E/Y$  and nearly equal to 3 as predicted by the rigid/plastic model (dashed-dotted line) [8]. At the smaller  $E/Y$  region, they are remarkably close to the prediction for  $\alpha = 1$ . This suggests that the plastic deformation in the core of metals and polymers is so uniform that the flat-die model would be applicable. It will also be justified from a different direction. According to the slip-line field solution for indentation by Hill ([8], p. 254), the plastic zone size in the rigid/plastic model is twice the indentation size. Equation 11 indicates that  $H_v/Y$  becomes almost 3 at  $b/c_1 = 2$  and  $\alpha = 1$ , being equal to the value of  $H_v/Y$  for rigid/

TABLE I Normalized modulus and hardness for ceramics ( $\sigma_B =$  tensile strength)

Materials	$E$ (GPa)	$H_v$ (GPa)	$\sigma_B$ (GPa)	$E/\sigma_B$	$H_v/\sigma_B$
$Al_2O_3$	421*	25.5*	20.6†	20.4	1.24
BeO	343*	12.7*	12.7†	27.0	1.00
$B_4C$	480*	23.5*	13.7†	35.0	1.72
SiC	480‡	24.0‡	20.6†	23.3	1.17
$Si_3N_4$	377‡	18.5‡	13.7†	27.5	1.35
Soda glass§	68.6	5.32	3.43	20.0	1.55

\*[22], †[21], ‡[3], §[15].

plastic model. This means that the elastic/plastic behaviour of ductile materials would continuously change to the rigid/plastic one as the plastic zone size approaches twice the indentation size with the increase in  $H_v/Y$ .

The results for ceramics seem to agree with the line  $\alpha = 1/3$ , although the data scatter rather widely. This suggests that the plastic deformation in the core of ceramics would occur inhomogeneously as it could do in the expansion of completely plastic spherical shell. It is also justified in the following. Johnson [9] indicates that the lower limit of  $p/Y$  should be the value of the elastic limit  $p/Y \cong 1$  or  $H_v \cong 0.93$ . This relation is represented in Fig. 2 as the lower boundary. For such extremely brittle materials as ceramics, the elastic/plastic solution would be intimately correlated with the elastic one [16, 23], and the elastic/plastic boundary in the present model would coincide with the boundary of the core ( $c_1/b = 1$ ) at  $p/Y = 1$ . From Equation 11, this yields  $\alpha = 1/3$ .

### 3.2. The plastic zone size

The experimental observations for the plastic zone size relative to half the indentation diagonal  $b/c$  are compared with Equation 9 for various  $\alpha$ -values as shown in Fig. 3. The theoretical plastic zone size is limited in the lower end by the boundary of the core ( $b = c_1 = 0.8c$ ). Most of the experimental results were elicited from Table I of Chiang *et al.* [4]; hot-rolled brass [24], cold-rolled steel [24], ZnS [25], KCl [26],  $Al_2O_3-ZrO_2$  [27] and soda lime glass [28, 29]. The remaining materials are quoted from the literature;  $(MnZn)Fe_2O_4$  [6, 30],  $Si_3N_4$  [31] and fused silica glass [28, 29]. Equation 9 is not strongly dependent on the parameter  $\alpha$ , and as a whole shows reasonable agreement with the observed relative plastic zone sizes. Particularly, it seems that the curve for  $\alpha = 1/3$  exhibits the best fitting in the lower  $E/H_v$  region.

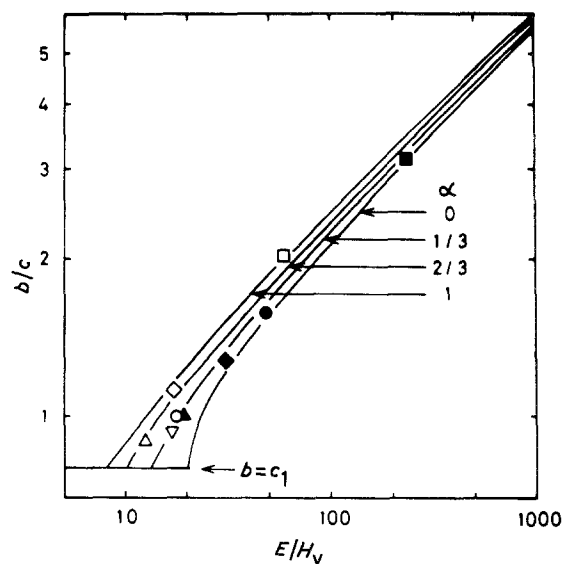


Figure 3 Literature data of experimental observations on the relative plastic zone size against the ratio of the modulus to the hardness for a range of materials. Also shown are predictions in the present analysis for four  $\alpha$ -values ( $\nu = 0.25$ ). ( $\blacksquare$ ) Hot-rolled brass, ( $\square$ ) cold-rolled steel, ( $\bullet$ ) ZnS, ( $\blacklozenge$ )  $(MnZn)Fe_2O_4$ , ( $\blacktriangle$ ) KCl, ( $\circ$ )  $Si_3N_4$ , ( $\diamond$ )  $Al_2O_3-ZrO_2$ , ( $\nabla$ ) Fused silica glass, ( $\Delta$ ) soda lime glass.

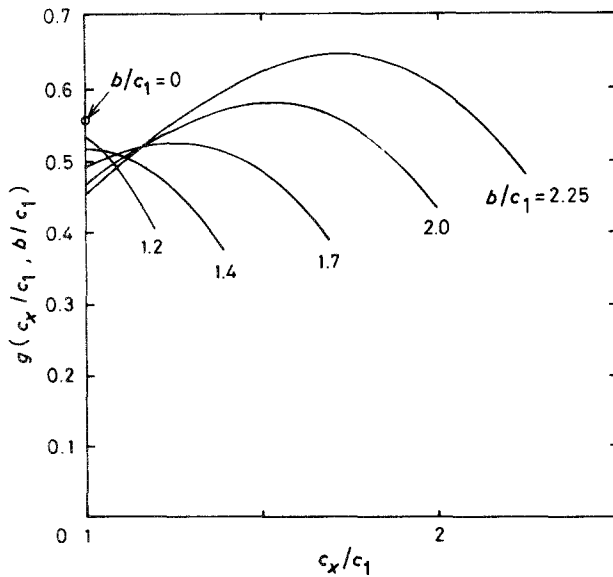


Figure 4 Plot of the function  $g$  in Equation 20 against  $c_x/c_1$  as a function of  $b/c_1$  ( $\nu = 0.25$ ).

Chiang *et al.* [4] calculated the elastic/plastic stress field from Equations 12 and 13 by replacing Johnson's incompressible core by an equivalent cavity, the volume of which is equal to the Vickers indentation volume. Thus the radius of the equivalent cavity,  $c'$ , is equal to  $0.45c$ . Modifying the pressure and yield stress to account for the pressure of a free surface, they insist that their analysis coincides with the experimental results on the contact pressure and the relative plastic zone size. However, the concept in their model had some confusion in the definition of hardness. As described in their companion work [5], hardness is defined in terms of the projected area;  $H_v = P/2c^2$ . They give an upper bound of the peak load stress field the hemispherical cavity solution relating the load to the indentation radius by  $P = p\pi c^2$ . Hence, according to their definition,  $H_v = p\pi c^2/2c^2 \cong 0.32p$ . They compare  $p$  directly with the experimental data as in their Fig. 1 [4]. This means that the comparison involves an error of a factor of three in the evaluation of hardness, and the modification by the free surface effect makes the error slightly larger.

It is noted that as the plastic zone size becomes comparable with the indentation size with the decrease in  $E/H_v$ , the prediction of the inclusion core model in the present work differs markedly from that of Johnson's incompressible core model [9] or the spherical cavity model [2, 4]. On the basis of the analysis of Lawn *et al.* [2], Chiang *et al.* [4] assumes the applicability of the one-half power dependency of  $b/c$  on  $E/H_v$  in the whole range of  $E/H_v$ . However, it is evident from Fig. 3 that the one-half power dependency may be a good approximation at high  $E/H_v$  values, while the dependency deviates to a much steeper one as  $E/H_v$  approaches the lower end.

### 3.3. The stress intensity factor

The stress intensity factor for well-developed cracks in the present model varies with the crack-opening location  $c_x$ . Fig. 4 represents the parameter  $g(c_x/c_1, b/c_1)$  in Equation 20 against  $c_x/c_1$  as a function of  $b/c_1$ . The analytical result indicates that the stress intensity factor  $K$  becomes maximum at the boundary of the core ( $c_x/c_1 = 1$ ) at the relatively small zone size ( $b/c_1 < 1.4$ ), while the maximized position moves to a location between the core and plastic zone boundary at the higher  $b/c_1$  values. It is probable that the equilibrium growth of the cracks occurs when the resulting maximum stress intensity factor  $K$  attains to the toughness  $K_c$ . Hence from the maximum values thus obtained, the correlation factors  $K/(P/a^{3/2})$  are computed for various  $\alpha$ -values using Equation 20, and plotted in Fig. 5 against the ratio of elastic modulus to yield stress. These curves are limited in the lower  $E/H_v$  region by the condition expressed in Equation 10. For reference, the correlation factor appropriate to the infinite body in the neglect of the free surface is calculated from Equation 18 for  $\alpha = 0$ , and plotted in the same figure. In this case the stress intensity factor is maximized at  $c_x = b$ . The comparison of the curve derived from Equation 20 for  $\alpha = 0$  with that from Equation 18 shows that the effect of a free surface reduces the correlation factor by about 50%.

Figure 5 demonstrates that, with the increase in the value of parameter  $\alpha$ , the correlation factors derived from Equation 20 decrease, while the dependency on

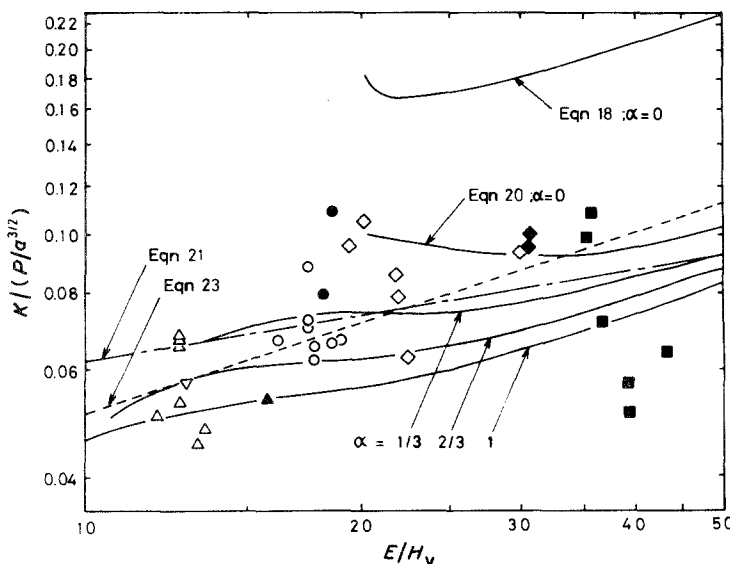


Figure 5 Correlation of experiments on normalized fracture toughness against the ratio of the modulus to the hardness for a range of materials. Also shown are the theoretical predictions from the present analysis ( $\nu = 0.25$ ), and the empirical relations from Tanaka [7] and Antis *et al.* [3]. (○)  $\text{Si}_3\text{N}_4$ , (●)  $\text{SiC}$ , (◇)  $\text{Al}_2\text{O}_3$ , (▽) glass-ceramic, (△) glass, (▲) Si, (◆)  $(\text{MnZn})\text{Fe}_2\text{O}_4$ , (■)  $\text{WC/Co}$ .

$E/H_v$  tends to increase. In particular, for the case where  $\alpha = 0$ , the correlation factor is almost independent of  $E/H_v$ . These theoretical results are compared with the experimental ones evaluated by the ratio of toughness values determined by the conventional methods to  $P/a^{3/2}$  values obtained by indentation, for various materials. Detailed information of most of the data from the literature is tabulated in Tanaka [7]. The newly quoted data in the present work are for WC/Co alloys [32] and  $Al_2O_3$  [12]. The theoretical curves show reasonable agreement with the general trend of the observed correlation factors, where the dependency on modulus-to-hardness appears very weak. Although the data scatter of experiments is large, it seems that the best fitting curve is the case of  $\alpha = 1/3$ , as also coincident with the results on the hardness in Fig. 2 and the plastic zone size in Fig. 3. The curve may be approximated by the straight dash-dotted line, which is expressed by

$$K_c = 0.035 (E/H_v)^{1/4} (P/a^{3/2}). \quad (21)$$

Tanaka [7] examined the correlation between the indentation-determined and conventional toughness available in the literature and concluded that  $K_c$  can be approximated independently of  $E/H_v$  with an accuracy within the data scatter as

$$K_c = 0.0725(P/a^{3/2}). \quad (22)$$

Lewis *et al.* [30] investigated the fracture of  $Si_3N_4$  ceramic alloys and also gave the same relationship with the appropriate constant of 0.073. Using the theoretical analysis proposed by Lawn *et al.* [2], Antis *et al.* [3] proposed that the correlation factor should depend on  $E/H_v$  to the one-half power, and then determined the ‘‘calibration’’ constant comparing the indentation-determined toughness values with the conventional ones:

$$K_c = 0.016(E/H_v)^{1/2} (P/a^{3/2}) \quad (23)$$

It is evident from the curve derived from Equation 18 that the one-half power dependency may be correct for an infinite body in the region with the  $E/H_v$  value higher than about 30. As seen in Fig. 5, Equation 21 lies between Equations 22 and 23 for the usual ceramics. This indicates that the present analysis gives a theoretical basis for these semi-empirical correlations.

#### 4. Conclusion

Elastic/plastic indentation has been calculated by allowing the indentation pressure to be transmitted via a misfitted inclusion core beneath the indenter. This core is compressible and replaces the incompressible core in Johnson’s model. The elastic field produced by the indentation has been evaluated by combining Eshelby’s spherical inclusion problem and Hill’s spherical-cavity expansion analysis. The plastic deformation inside and outside the inclusion core ensures the compatibility between the volume of a material displaced by the indenter and that accommodated by expansion. It is assumed that the applied load is balanced with the internal stress field in addition to the stress,  $\alpha Y$ , required for the plastic work dissipated in the core. The analysis indicates that essential

relationships between the indentation plasticity and the dominant material properties: yield stress, hardness, elastic modulus, and Poisson’s ratio. Predictions of the hardness/yield stress ratio with the elastic modulus/yield stress ratio have been shown to correlate with the experimental results for metal and polymers by  $\alpha = 1$  and ceramics by  $\alpha = 1/3$ . Similarly, predictions of the plastic-zone dimension in terms of the hardness and elastic modulus agree well with experimental observations for a wide range of materials.

The solution has been used to evaluate the indentation fracture toughness, accounting for the image force contribution from the presence of the free surface. Predictions of the correlation factor  $K/(P/a^{3/2})$  with the elastic modulus/hardness ratio correspond the most closely to the trends demonstrated by the available experimental data when  $\alpha = 1/3$ .

#### Acknowledgements

The detailed information offered by Drs S. Muneki and Y. Kawabe, NRIM, for their data on hardness and strength of maraging steels is greatly acknowledged.

#### Appendix 1. Evaluation of indentation volume change

Let us consider a case of an expanding spherical cavity with its internal radius of  $c_1$  under internal pressure  $p_2$  in an infinite medium. The stresses and displacements in the elastic/plastic region outside the cavity are taken from Hill [8], whence the current total internal radius of the cavity  $c_1 + u$  is given by

$$(c_1 + u)^3/c_1^3 = 1 + 3(1 - \nu)Yb^3/Ec_1^3 - 3(1 - 2\nu)p_2/E \quad (A1)$$

([8], p. 101, Equation 14). If the cavity is stressed elastically (reversibly) under the same pressure, the radial displacement of the internal radius of the cavity  $u_e$  will be given by

$$u_e = p_2(1 + \nu)c_1/2E \quad (A2)$$

([8], p. 98, Equation 2). Under the condition that the radial displacements  $u$  and  $u_e$  are negligibly small compared to the initial radius  $c_1$ , the irreversible (plastic) volume change of the cavity  $\Delta V_2$  is evaluated from Equations A1 and A2 as

$$\Delta V_2 = 4\pi(u - u_e)c_1^2 = 4\pi(1 - \nu)Yb^3/E - 6\pi(1 - \nu)p_2c_1^3/E. \quad (A3)$$

Dividing both sides of Equations A3 by  $4\pi c_1^3/3$ , we can obtain the relation in Equation 2.

#### Appendix 2. Stress analysis for the surface stresses

On the assumption of the spherical inclusion, the internal stresses becomes axisymmetric. Hence, the case where a uniform traction  $\sigma_t(\varrho)$  is distributed over the area on a free surface  $x_3 = 0$  between the radii  $\varrho$  and  $\varrho + d\varrho$  (Fig. A1) is considered. The stress  $\sigma_{22}(r, \phi, \varrho)$  at a point  $(x_1, 0, x_3)$  is calculated by the superposition of Mindlin’s solution [13, 14] for a concentrated force  $\sigma_t(\varrho)\varrho d\varrho d\theta$  applied at a point  $(\varrho \cos \theta,$

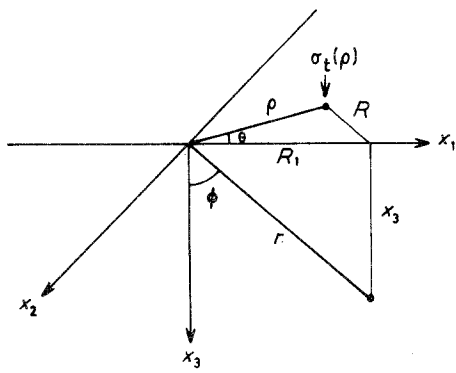


Figure A1 Coordinate system used for stress analysis.

$\rho \sin \theta, 0$ ) in the positive  $x_3$  direction as

$$\sigma_{22}(r, \phi, \rho) = \rho d\rho \int_0^{2\pi} \sigma_{22}(r, \phi, \rho, \theta) d\theta \quad (\text{A4})$$

where

$$\begin{aligned} \sigma_{22}(r, \phi, \rho, \theta) = & - [\sigma_t(\rho)/2\pi] \{ (1 - 2\nu)[\rho^2 \sin^2 \theta \\ & - (R_1 - \rho \cos \theta)^2]/R^4 - (1 - 2\nu)x_3[\rho^2 \sin^2 \theta \\ & - (R_1 - \rho \cos \theta)^2]/R^4(R^2 + x_3^2)^{1/2} \\ & - 3x_3\rho^2 \sin^2 \theta/(R^2 + x_3^2)^{5/2} \\ & + (1 - 2\nu)x_3(R_1 - \rho \cos \theta)^2/R^2(R^2 + x_3^2)^{3/2} \}. \end{aligned}$$

Here  $r = (x_1^2 + x_3^2)^{1/2}$ ,  $R = (\rho^2 - 2R_1\rho \cos \theta + R_1^2)^{1/2}$  and  $R_1 = r \sin \phi$ ,  $x_3 = r \cos \phi$ . The stress  $\bar{\sigma}_{22}(r, \rho)$  at a radial location  $r$  from the crack centre averaged over the angular range is determined by

$$\bar{\sigma}_{22}(r, \rho) = (1/\pi) \int_0^\pi \sigma_{22}(r, \phi, \rho) d\phi. \quad (\text{A5})$$

The analytical solution for Equation A5 is extremely complicated, and thus Equation A5 is numerically integrated for the case where  $\nu = 0.25$ . The result is given in a form,

$$\sigma_{22}(r, \rho) = -[\sigma_t(\rho)d\rho/\pi\rho]f(r/\rho) \quad (\text{A6})$$

The function  $f(r/\rho)$  is indicated by a solid curve in Fig. A2 against  $r/\rho$ . The approximate analytic solution for  $f(r/\rho)$  is obtained by a polynomial,

$$f(r/\rho) = u_1(r/\rho) + u_3(r/\rho)^3 + u_5(r/\rho)^5, \quad r/\rho \leq 1$$

with

$$\begin{aligned} u_1 = & -5/2, \quad u_3 = 51/16, \quad u_5 = -153/64 \\ f(r/\rho) = & v_3(\rho/r)^3 + v_4(\rho/r)^4 + v_5(\rho/r)^5 + v_6(\rho/r)^6 \\ & + v_7(\rho/r)^7, \quad r/\rho > 1 \end{aligned} \quad (\text{A7})$$

with

$$\begin{aligned} v_3 = & -1, \quad v_4 = -2.5, \quad v_5 = -0.5, \quad v_6 = 6, \\ v_7 = & -6.6 \end{aligned}$$

This is given by the dotted curves in Fig. A2. The approximate solution agrees well with the numerical solution except in the case where  $r/\rho$  approaches very closely to one. Integration of Equation A6 after the substitution of  $-\bar{\sigma}_{33}(\rho)$  into  $\sigma_t(\rho)$  yields Equation 19.

## References

1. B. R. LAWN and T. R. WILSHAW, *J. Mater. Sci.* **10** (1975) 1049.
2. B. R. LAWN, A. G. EVANS and P. B. MARSHALL, *J. Amer. Ceram. Soc.* **63** (1980) 574.
3. G. R. ANTIS, P. CHANTIKUL, B. R. LAWN and D. B. MARSHALL, *ibid.* **64** (1981) 533.
4. S. S. CHIANG, D. B. MARSHALL and A. G. EVANS, *J. Appl. Phys.* **53** (1982) 298.
5. *Idem, ibid.* **53** (1982), 312.
6. K. TANAKA, Y. KITAHARA, Y. ICHINOSE and T. HIMURA, *Acta Metall.* **32** (1984) 1719.
7. K. TANAKA, *Nihon Kinzoku Gakkaishi* **48** (1984) 1157 (in Japanese).
8. R. HILL, "The Mathematical Theory of Plasticity" (Oxford University Press, London, 1950).
9. K. JOHNSON, *J. Mech. Phys. Solids* **18** (1970) 115.
10. J. D. ESHELBY, *Proc. Roy. Soc.* **A241** (1957), 376.
11. *Idem, ibid.* **A252** (1959), 561.
12. K. TANAKA, *Scripta Metall.* **19** (1985) 1183.
13. R. D. MINDLIN, *Physics* **7** (1936) 85.
14. S. TIMOSHENKO and J. N. GOODIER, "Theory of Elasticity" (McGraw-Hill, New York, 1951).
15. D. M. MARSH, *Proc. Roy. Soc.* **A279** (1964) 420.
16. W. HIRST and M. G. J. W. HOWSE, *ibid.* **A211** (1969) 492.
17. S. NISHIJIMA, *Trans. NRIM* **19** (1977) 327.
18. *Idem, ibid.* **20** (1978) 314.
19. NRIM Fatigue Data Sheet, National Research Institute for Metals, Tokyo, Japan, no. 1-4, (1978), no. 8-10 (1979).
20. S. MUNEKI, Y. KAWABE, K. NAKAZAWA and H. YAJI, *Tetsu-to-Hagane* **64** (1978) 605 (in Japanese).

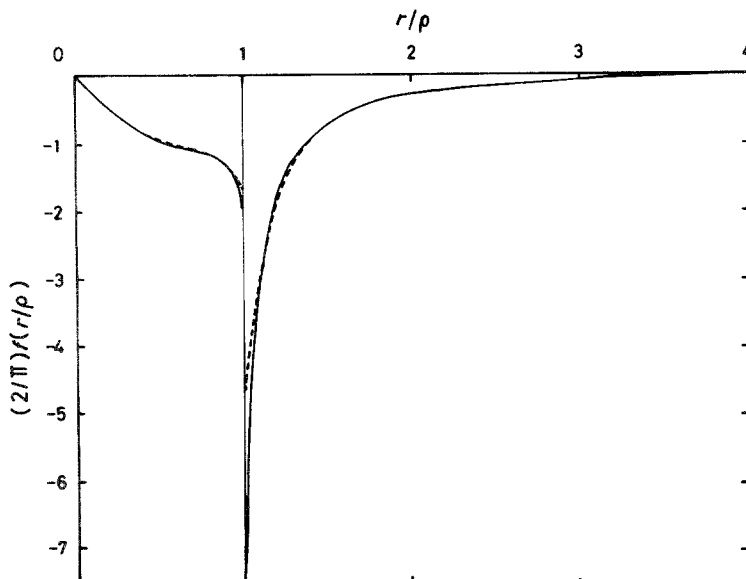


Figure A2 Plot of the function  $f(r/\rho)$  in Equation A6 against  $r/\rho$ . (—) Numerical integration, (---) approximation.

21. W. H. SUTTON, *Astronautics and Aeronautics (AIAA)* August (1966) 46.
22. A. KELLY "Strong Solids" (Oxford University Press, 1966).
23. C. M. FERROTT, *Wear* **45** (1977) 293.
24. T. O. MULHEARN *J. Mech. Phys. Solids* **7** (1959) 85.
25. S. VAN DER ZWAAG, J. T. HAGA and J. E. FIELD, *J. Mater. Sci.* **15** (1980) 2965.
26. J. T. HAGAN, *ibid.* **14** (1979) 2975.
27. N. H. BURLINGAME, M S Thesis, University of California, Berkley, (1980).
28. J. T. HAGAN, *J. Mater. Sci.* **14** (1979) 462.
29. *Idem, ibid.* **15** (1980) 1417.
30. K. TANAKA, unpublished work, 1985.
31. M. H. LEWIS, R. FUNG and D. M. R. TAPLIN, *J. Mater. Sci.* **16** (1981) 3437.
32. E. L. EXNER, J. R. PICKENS and J. GURLAND, *Met. Trans.* **9A** (1978) 736.

*Received 9 June  
and accepted 18 August 1986*